Shear and Extensional Properties of Three-Arm Polystyrene Solutions

Xiangnan Ye and Tam Sridhar*

Department of Chemical Engineering, Monash University, Clayton, Australia 3180

Received December 26, 2000; Revised Manuscript Received November 15, 2001

ABSTRACT: Following the impressive advances in understanding the rheology of linear polymers using the basic Doi−Edwards model of reptation and its variants, rheologists are turning their attention to branched polymers. This is primarily motivated by a desire to understand the connection between chain topology and rheology. We examine the behavior of star polymers in shear and extensional flows. We use this study to illustrate the dramatic effect that the branch point has on both shear and extension. Data on steady and oscillatory shear and step strain shear are presented and analyzed using the Milner−McLeish model. Excellent agreement, using a consistent parameter set, is obtained between this theory and experiments. The filament-stretching rheometer is used to obtain the extensional viscosity of these solutions. The steady-state extensional viscosity shows strain rate softening at moderate strain rates and strain rate hardening at high strain rates. At low Weissenberg numbers (based on the longest relaxation time), the steady extensional stress depends on the number of chain entanglements. At the other extreme, at high Weissenberg number (based on the Rouse time), the steady-state stress depends only on the Weissenberg number. Qualitative similarities and some differences with linear polymers are noticed. The differences appear to be related to the different time constants for the longest relaxation times in these systems.

Introduction

In concentrated solutions or melts of linear polymers, the Doi−Edwards reptation theory assumes that a molecule is surrounded by other molecules, whose effect can be considered as a constraining tube.[1] In the past few decades, this theory has been remarkably successful in describing the viscoelastic behavior for concentrated solutions and melts of linear polymers. The major mechanisms of relaxation in this model include reptation and fluctuation of the chain within the constraining tube and the release of constraints by the motion of the surrounding molecules. For star polymers, where many branches connect to a central point, reptation is suppressed, and relaxation occurs by a combination of fluctuation plus constraint release. Thus, the reptation of linear chain is replaced by "arm retraction". That is, the free ends of the star branches retract back along the "arm confining tube" and then seek out new directions.[2] The retraction can be considered as a particle diffusing through a potential well $U(s)$, which depends exponentially on the distance from the free end of arm. Such models describe the rheological properties of star polymer melts, and the predictions are in good agreement with experiments.[3−5] In principle, only two parameters are needed in these models, i.e., number of entanglements Z and the Rouse relaxation time of a segment τ_e.

Much of the published research has been focused on shear rheology of star melts. Extensional data for star polymer solutions are not available. Recent advances in extensional rheometry make such measurements possible using the constant-stretch-rate technique, which was developed by Sridhar and co-workers.[6,7] Details of this development can be found in Gupta et al.[8] and Anna et al.[9] In this work, we use this rheometer to investigate the extensional behavior of star polymer solutions. Three-arm star polymers at different concentrations are examined. Measurements using steady shear, oscillatory flow, and step strain experiments enable the fluids to be fully characterized and evaluate the time constants. The extensional data are then examined using these time constants. Finally, some comparison is presented between star and linear polymers in extension.

Theoretical Background

Pearson and Helfand considered the relaxation for a single star polymer in a fixed network.[3] They pointed out that the arm retraction could be represented as movement in a potential U_1 given by

$$U_1(s) = \frac{3Z}{2} s^2 \tag{1}$$

where s is the dimensionless distance from the free end along the tube and Z is the number of entanglements per arm, which is the ratio of numbers of monomers in the chain to the numbers of monomers in an entanglement segment, N_e. The time scale for the retraction is

$$\tau(s) = \tau_0 \exp[U_1(s)] \tag{2}$$

A simple approach suggests taking τ_0 as the Rouse time τ_R with

$$\tau_R = \tau_e Z^2 \tag{3}$$

where τ_e is the Rouse time of an entanglement segment. The relaxation function can be expressed as

$$G(t) = 2G_N^0 \int_0^1 ds\ (1 - s) \exp\left(-\frac{t}{\tau(s)}\right) \tag{4a}$$

or after applying the Fourier transform as

$$G(\omega) = 2G_N^0 \int_0^1 ds\ (1 - s)\left[\frac{i\omega\tau(s)}{1 + i\omega\tau(s)}\right] \tag{4b}$$

Ball and McLeish recognized that the relaxation spectrum of a star chain in the melt state is influenced by the mobility of other chains.[4] Because of the broad

10.1021/ma002192o CCC: $20.00
Published on Web 10/04/2001

spectrum of relaxation times, portions of the chain near the branch point perceive the free ends to be mobile. As a result, some of the entanglements are not effective, and N_e reduced by this dynamic dilution is given by

$$N_e(\Phi) = \frac{N_e}{\Phi} \tag{5}$$

where $\Phi = 1 - s$ is the volume fraction of unrelaxed arm segment. The process of dynamic dilution gives rise to an activation energy.

$$U_2(s) = \frac{3Z}{2}\left(s^2 - \frac{2s^3}{3}\right) \tag{6}$$

Compared with eq 1, the potential $U_2(s)$ is reduced by a factor of 3 at $s = 1$. The time scales then follow according to eq 2.

Milner and McLeish have suggested several improvements to the Ball−McLeish model. They have identified two regimes of relaxation processes.[5] The early relaxation of segments near the free end is not influenced by the branch point. However, segments near the branch point are activated, and an approximate expression is proposed for the crossover between these two regimes. In addition, Milner and McLeish incorporate the scaling arguments of Colby and Rubinstein[10] for the concentration dependence of the entanglement length.

According to the Ball−McLeish model, $N_e(\Phi) = N_e/\Phi$ will result in the following scaling:

$$G(\Phi) \sim G_N^0 \Phi^2 \tag{7}$$

Such a result does not agree with the experimental data for θ solutions. Colby and Rubinstein[10] assumed that entanglements are binary events between chains which, in θ solutions, leads to the scaling

$$N_e(\Phi) = N_e \Phi^{-\alpha} \tag{8}$$

where $\alpha = {}^4/_3$. This assumption implies $G(\Phi) \sim G_N^0 \Phi^{7/3}$, which appears to be in good agreement with the θ solution data.[5] In what follows, we use $\alpha = {}^4/_3$ for the calculations presented in this paper.

The activation barrier for the Milner−McLeish model is given as

$$U(s) = 3Z\,\frac{1 - (1 - s)^{1+\alpha}[1 + (1 + \alpha)s]}{(1 + \alpha)(2 + \alpha)} \tag{9}$$

and the relaxation function is

$$G(t) = (1 + \alpha)G_N^0 \int_0^1 \mathrm{d}s\,(1 - s)^\alpha \exp\left(-\frac{t}{\tau(s)}\right) \tag{10a}$$

or after applying the Fourier transform as

$$G(\omega) = (1 + \alpha)G_N^0 \int_0^1 \mathrm{d}s\,(1 - s)^\alpha \left[\frac{i\omega\tau(s)}{1 + i\omega\tau(s)}\right] \tag{10b}$$

Notice that eqs 9 and 10 reduce to eqs 6 and 4 when $\alpha = 1$. For the retraction of free ends within a small distance s, the potential function $U(s)$ is unimportant, and thus the ends can move freely without any influence of the junction point. The Rouse model can be applied for this regime, and the time scale is given by[5]

$$\tau_{early}(s) = \frac{9\pi^3}{16} Z^4 \tau_e s^4 \tag{11}$$

For longer times, arm retraction is an activated process. Milner and McLeish gave an approximate expression for the time scale by solving a first passage time problem[5,11]

$$\tau_{late}(s) = \tau_e \sqrt{\frac{\pi^5 Z^3}{6}} \times \frac{\exp[U(s)]}{\left[s^2(1 - s)^{2\alpha} + \left[\left(\frac{1}{3Z}\right)(1 + \alpha)\right]^{2\alpha/(1+\alpha)} \Gamma\left(\frac{1}{1 + \alpha}\right)^{-2}\right]^{1/2}} \tag{12}$$

Finally, a simple expression was presented for the crossover between the contributions of Rouse motion and activated arm retraction, i.e.

$$\tau(s) = \frac{\tau_{late}(s)\,\tau_{early}(s)\,\exp[U(s)]}{\tau_{late}(s) + \tau_{early}(s)\,\exp[U(s)]} \tag{13}$$

where $\tau_{early}(s)$ and $\tau_{late}(s)$ are given by eqs 11 and 12, respectively.

The only parameters appearing in this model are the number of entanglements per arm Z, the plateau modulus G_N^0, and the Rouse time of a segment τ_e.[11] The plateau modulus is related to the number of entanglements through the molecular weight between entanglements, and hence the number of parameters is reduced to two. In principle, these parameters can be obtained using methods established for linear polymers with the same molecular weight as the arm chain. Recently, this model has been tested using rheological data on star polymer melts,[5] the star−star blend system,[12] and the star−linear blend systems[13] and found to describe such data well.

Experimental Section

The three-arm polystyrene (PS) used in this study was purchased from Polymer Source Inc. (Canada). The molecular weight of the polymer and the molecular weight of the arms were determined by light scattering and size exclusion chromatography by the suppliers. Four concentrated solutions were prepared by dissolving the star polymer in di-*n*-butyl phthalate (DBP), which is a good solvent for polystyrene. Both PS and DBP were dissolved in a large amount of methylene chloride and mixed for at least 24 h to ensure that the solutions were homogeneous. Methylene chloride was later completely evaporated in a vacuum oven over a few days until no further weight loss was registered. The physical properties and other relevant data for the solutions are provided in Table 1.

The steady shear and dynamic data of these solutions were measured with a Rheometrics fluid spectrometer (RFS II). All measurements are performed in the linear regime using the cone−plate geometry (50 mm in diameter and a gap angle of 0.04 rad). For each solution, rheological data are obtained at

Table 1. Physical Characteristics of the Star Polystyrene Solutions Used in the Study

polymer	M_w stark, g/mol	M_n arm, kg/mol	PI[a]	wt fraction, wt %	vol fraction	η_0,[b] Pa·s	η_0,[c] Pa·s
3-arm PS	3470	1116	1.08	10	0.098	340	336
				12	0.118	1135	1140
				15	0.147	8850	8739
				20	0.196	35000	38600

[a] Polydispersity index (M_w/M_n). [b] Obtained from dynamic viscosity in the low-frequency region. [c] Calculated from eq 24.

three different temperatures. We choose 21 °C as the reference temperature, T_0, and the data are shifted to this temperature. The shift factor was obtained from the zero-frequency dynamic viscosity,

$$a_T = \frac{\eta_0'|_T}{\eta'_0|_{T_0}} \tag{14}$$

We also assume that the temperature dependence of all properties is given by the same shift factor a_T. Thus, the following parameters are defined to describe the master curves at the reference temperature: T_0

$$\omega|_{T_0} = a_T\omega|_T \qquad \eta|_{T_0} = \eta|_T/a_T \tag{15}$$

$$\dot\gamma|_{T_0} = a_T\dot\gamma|_T \qquad N_1|_{T_0} = N_1|_T \tag{16}$$

$$G'(\omega|_{T_0}) = G'(\omega|_T) \qquad G''(\omega|_{T_0}) = G''(\omega|_T) \tag{17}$$

In addition, step strain experiments are also carried out with RFS II at 21 °C. The imposed strains varied from 1% to 100%. At the lower strains (up to 10%), the relaxation modulus was independent of the imposed strain and hence was used to measure the relaxation modulus $G(t)$.

The filament stretching technique was used to conduct the extensional stress growth measurements. For ideal extension, the length and mid-filament diameter of the filament are governed by the following equations:

$$L = L_0 \exp(\dot\epsilon t) \tag{18}$$

$$D = D_0 \exp(-\dot\epsilon t/2) \tag{19}$$

where $\dot\epsilon$ is the extensional rate; L_0 and D_0 are initial length and diameter of the filament, respectively. However, because of the end effects, it is impossible to satisfy both these equations simultaneously. As described by Tirtaatmadja and Sridhar, the mid-filament diameter will decrease more rapidly than expected.[6] To obtain a constant stretch rate based on the diameter, the velocity profile needs to be changed. A "master plot" technique was applied to impose a constant and predetermined strain rate.[8,9] The actual strain rates calculated from the slope of the diameter profile are within 10% of the imposed strain rates. Experimentally, entangled polymer solutions present two major challenges for filament stretching rheometer. Sample loading to achieve a uniform cylinder without entraining air bubbles is a difficult and time-consuming process due to the long relaxation times. In addition, filament breakage limits the maximum strain that can be achieved, while inhomogeneous stretching sets a lower limit on the strain rate that can be used. However, between these limits, the technique was reliable and gave reproducible results.

Results and Discussion

Shear and Dynamic Data. Figure 1 shows the master curves of shear viscosity (η) and first normal stress difference (N_1) for a typical solution. The shear stress increases monotonically with shear rate. At low shear rates, the normal stresses depend quadratically on the shear rate. To demonstrate the validity of the Cox−Merz rule,[14] we show shear viscosity (filled symbols) and the dynamic viscosity (open symbols) for 10 and 12 wt % solution at 21 °C in Figure 2. This empiricism has been proved to be valid for four-arm star polybutadiene solution[15] and three-arm star poly(isobutyl vinyl ether).[16] Values of zero shear viscosity η_0 obtained from dynamic viscosity in the low-frequency region are listed in Table 1. The dependence of η_0 on concentration (volume fraction ϕ) is similar to the

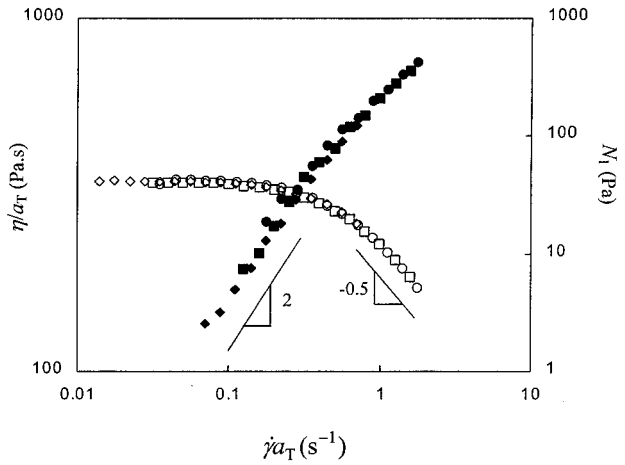

Figure 1. Master curves of shear viscosity (open symbols) and first normal stress difference (filled symbols) for 10 wt % solution. Diamonds, squares, and circles denote data at 30, 21, and 16 °C, respectively. The dashed lines have a slope of −0.5 and 2.

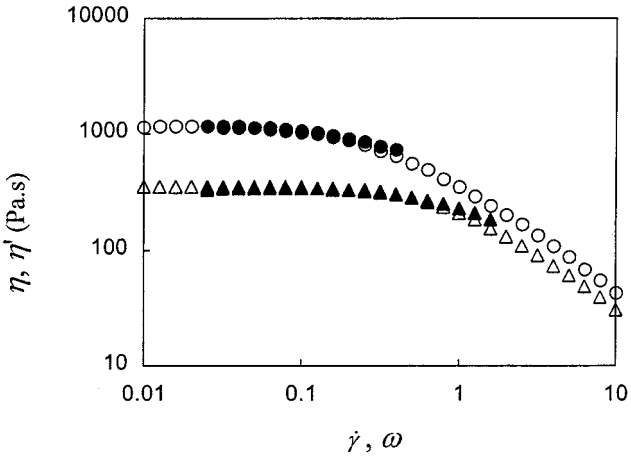

Figure 2. Comparison of steady-state shear viscosity (filled symbols) and dynamic viscosity (open symbols) for 10 wt % solution (triangles) and 12 wt % solution (circles) at 21 °C.

published data for four-arm polybutadiene solutions in a good solvent[17] and four-arm and six-arm polyisoprene solutions.[18] The master curves for storage and loss moduli, $G'(\omega)$ and $G''(\omega)$, for these four solutions are shown in Figures 3 and 4, respectively. The loss modulus for 10 wt % solution gives a shallow peak within the frequency range investigated. However, the maxima become much more obvious as the concentration increases.

Evaluation of Parameters. The Milner−McLeish model requires the following parameters: Z, G_N^0, and τ_e. In principle, Z and G_N^0 are dependent on each other and could be determined apriori from linear polystyrene samples. As a result, the Milner−McLeish model is essentially a one-parameter model. The entanglement molecular weight in a solution is given by

$$M_e^{soln} = M_e^{melt}\frac{\rho}{c} \quad c \geq 0.1\ \text{g/cm}^3 \tag{20}$$

where ρ is density of polymer, c is concentration of polymer, and M_e^{melt} is molecular weight between entanglements, which was taken as 13 300 for polystyrene melts.[19] Consequently, the number of entanglements of

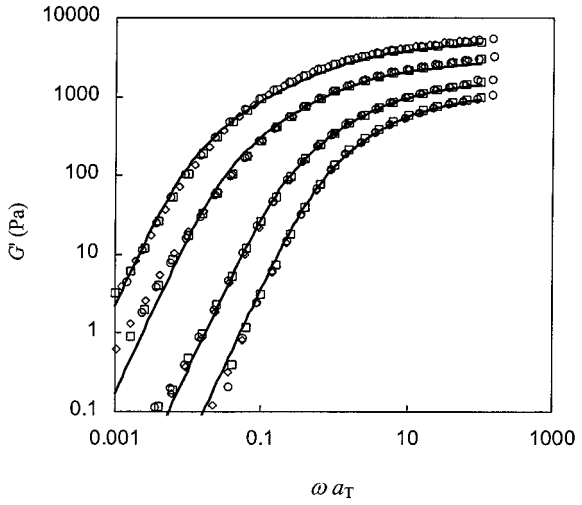

Figure 3. Master curves of storage modulus $G'(\omega)$. Concentrations from right to left are 10, 12, 15, and 20 wt %. Diamonds, squares, and circles denote data at 30, 21, and 16 °C, respectively. Solid lines are the Milner−McLeish model predictions.

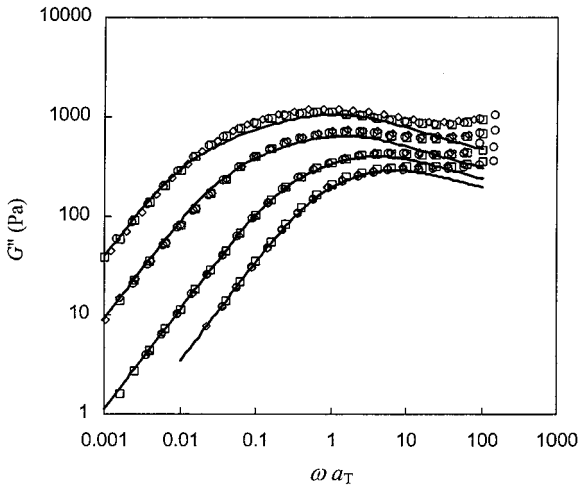

Figure 4. Master curves of loss modulus $G''(\omega)$. Concentrations from right to left are 10, 12, 15, and 20 wt %. Diamonds, squares, and circles denote data at 30, 21, and 16 °C, respectively. Solid lines are the Milner−McLeish model predictions.

the branches can be obtained by

$$Z = \frac{M_a}{M_e^{soln}} \tag{21}$$

where M_a is molecular weight of the arm.

The plateau modulus G_N^0 for the solutions can be determined experimentally from the storage modulus. However, the experimental data do not show a well-defined plateau to make an accurate estimation. Alternately, the value of M_e^{soln} can be used to obtain the G_N^0 based on the definition of entanglement molecular weight M_e^{soln}, i.e.

$$G_N^0 = \frac{4}{5}\frac{\rho\phi RT}{M_e^{soln}} \tag{22}$$

where ϕ is the volume fraction of the solution. The values of G_N^0 obtained from above equation are listed in Table 2.

The remaining model parameter is Rouse time of an entanglement segment τ_e, which is defined as[1]

$$\tau_e = \frac{\zeta N_e^2 b^2}{3\pi^2 k_B T} \tag{23}$$

where b is the effective bond length defined as $b = (M_0\langle R^2\rangle/M)^{1/2}$ and ζ is the monomeric friction constant. However, there are difficulties in the calculation of the end-to-end distance $\langle R^2\rangle$ and ζ for solutions. In this paper, we choose to calculate Z using eq 21 and determine the other two by fitting the experimental oscillatory data to the model. The predictions of the Milner−McLeish theory are shown as solid lines in Figures 3 and 4. The values of G_N^0 and τ_e have been obtained by fitting the experiments, and these are listed in Table 2. For all solutions, the values of G_N^0 required to get a good fit with experiments are within 10% of the value calculated from eq 22, confirming that the theory affords a one-parameter description of the relaxation process in star polymers. We notice that prediction of the Milner−McLeish theory is in good agreement with the experimental data for almost the full frequency range. A slight deviation between the model and experiments was found at high frequencies where higher order Rouse modes become important but are neglected in this model. This is perhaps, the first direct comparison of the Milner−McLeish model for solutions of star polymers.

Finally, it is interesting to calculate the longest relaxation time τ_1 from the Milner−McLeish model. This can be obtained from eq 13 with $s = 1$, which corresponds to the time required for the free end to retract back to the branch point. The values of τ_1 are also listed in Table 2. If the polymer chains were not constrained by the branch point, they would be able to reptate like a linear chain with a time constant $\tau_D = 3\tau_R Z = 3\tau_e Z^3$. Values of τ_D are also listed in Table 2 for comparison. Note that τ_1 is 20−150 times greater than τ_D. This dramatically illustrates the inefficiency of retraction as the relaxation mechanism compared to reptation. The effect of chain topology on the solution rheology is related to these significant changes in relaxation times.

Linear Viscoelasticity. The zero shear viscosity can also be obtained from relaxation modulus, i.e.

$$\eta_0 = \int_0^\infty G(t)\,dt \tag{24}$$

Thus, using the expression of $G(t)$ from the Milner−McLeish model, we can calculate the zero shear viscosity for these solutions, which are also listed in Table 1. These are in excellent agreement with experimental values. The Milner−McLeish model does not yield an analytical relationship between η_0 and τ_1. Figure 5 shows η_0/τ_1 calculated using the Milner−McLeish model as a function of the number of entanglements Z. Over a range of Z values from 10 to 25, a simple power law relationship is obtained:

$$\frac{\eta_0}{\tau_1} = 21.6Z^{0.83} \tag{25}$$

We shall later use this relationship to examine extensional data.

The relaxation modulus following a sudden imposition of shear can be factored into strain-dependent and time-

Table 2. Viscoelastic Data at 21 °C for the Star Polystyrene Solutions Used in the Study

concn, wt %	Z	τ_e,[a] s	τ_R,[a] s	τ_D,[a] s	τ_1,[b] s	G_N^0,[a] Pa	G_N^0,[c] Pa
10	8.4	8.0×10^{-5}	5.6×10^{-3}	0.14	2.8	1500	1461
12	10.1	8.0×10^{-5}	8.1×10^{-3}	0.25	7.8	2100	2107
15	12.6	1.2×10^{-4}	1.9×10^{-2}	0.72	49.1	3500	3299
20	16.8	8.2×10^{-5}	2.3×10^{-2}	1.16	150.5	6000	5886

[a] Obtained by fitting the Milner−McLeish theory to experimental data; τ_D is the reptation time for linear polymer with same molecular weight as the star polymer. [b] Longest relaxation time calculated from eq 13 with $s = 1$. [c] Calculated from eq 22.

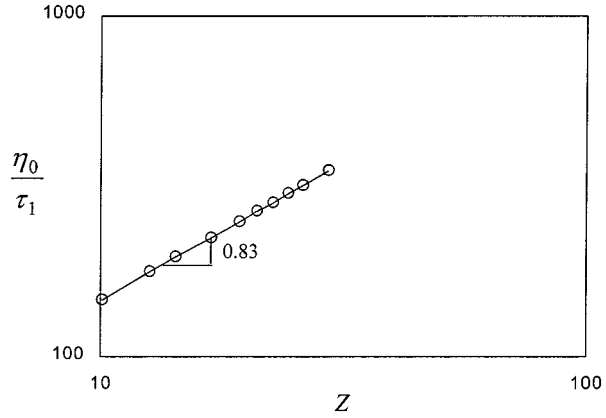

Figure 5. Simulated data for η_0/τ_1 using the Milner−McLeish model as a function of Z. The slope of the line is 0.83.

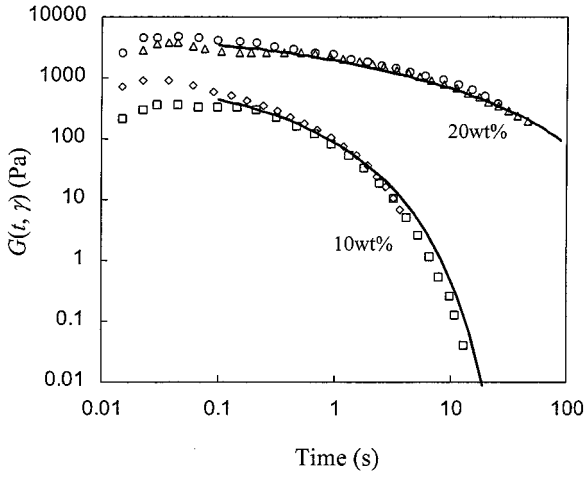

Figure 6. Shear relaxation modulus as a function of time at a representatively high strain ($\gamma = 100\%$, squares for 10 wt % solution; $\gamma = 12\%$, triangles for 20 wt % solution) and a low strain ($\gamma = 1\%$, diamond and circles for both solutions). Solid lines are the Milner−McLeish model prediction.

dependent function, that is, $G(t,\gamma) = h(\gamma)G(t)$ where the function $h(\gamma)$ is the damping function.[1] In the small strain region, the relaxation function becomes strain independent. Figure 6 shows the variation of the relaxation modulus with time for the 10 and 20 wt % solution at two representative shear strains. It is apparent that the curves are independent of the strain which suggests that under these conditions the damping function $h(\gamma) \approx 1$ and $G(t,\gamma) = G(t)$. The Milner−McLeish relaxation modulus is also shown as solid line in Figure 6. The relaxation modulus obtained from the dynamic data agrees well with the modulus evaluated from step strain experiments.

In summary, the relaxation modulus obtained from the Milner−McLeish model are in excellent agreement with steady shear, oscillatory, and step strain measurements and hence provide a useful basis for examining extensional data.

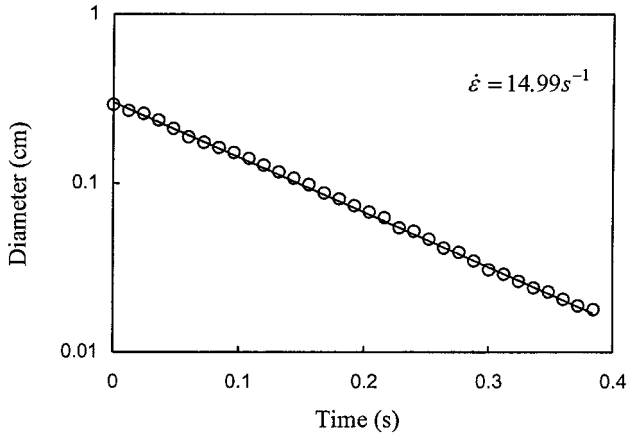

Figure 7. Diameter as a function of time for 10 wt % solution after applying "master plot" technique. An actual extensional rate of 14.99 s^{-1} (circles) was obtained when the imposed strain rate was 15.0 s^{-1}. The solid line shows the prediction of eq 19.

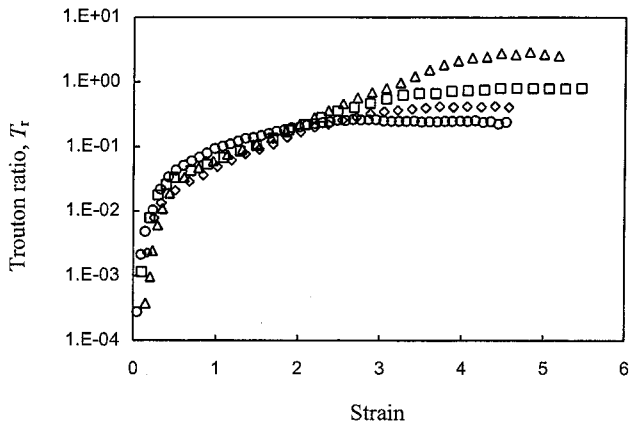

Figure 8. Trouton ratio as a function of strain for 20 wt % solution. Circles, diamonds, squares, and triangles denote the strain rates of 5, 8.5, 10, and 15 s^{-1}, respectively.

Extensional Data. Over a range of strain rates, star polymer solutions could be subject to constant and uniform extensional deformation. Figure 7 shows a typical diameter profile for the 10 wt % solution. The actual extensional rate obtained by applying the "master plot" technique[8,9] is within 10% of the imposed strain rate. The extensional stress growth coefficients, plotted as the Trouton ratio vs strain, are shown in Figure 8. The Trouton ratio is defined as the ratio of extensional viscosity to the zero shear viscosity,

$$T_r^+ = \frac{\eta_E^+}{\eta_0} \tag{26}$$

η_E^+ and T_r^+ are the time-dependent extensional viscosity and Trouton ratio. After a certain strain, the Trouton ratio reaches a steady state T_r. It is interesting to compare these results with those for dilute solutions (Boger fluids) of linear polystyrene presented by Gupta

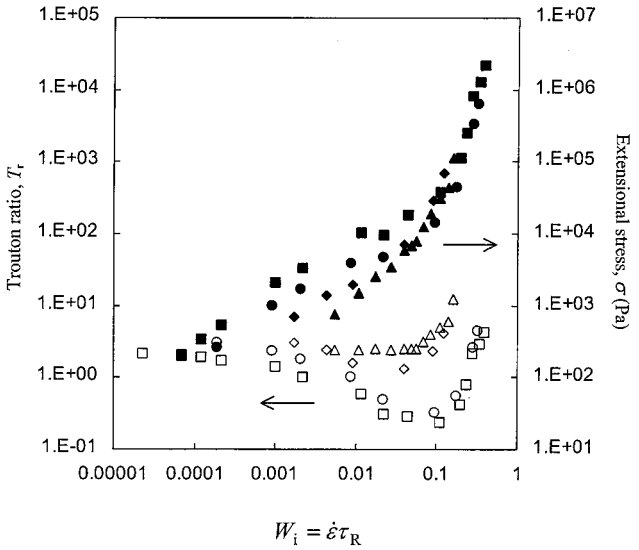

Figure 9. Trouton ratio (open symbols) and extensional stresses (filled symbols) as a function of Weissenberg number ($W_i = \dot{\epsilon}\tau_R$) for 10 wt % (triangles), 12 wt % (diamonds), 15 wt % (circles), and 20 wt % (squares) solutions.

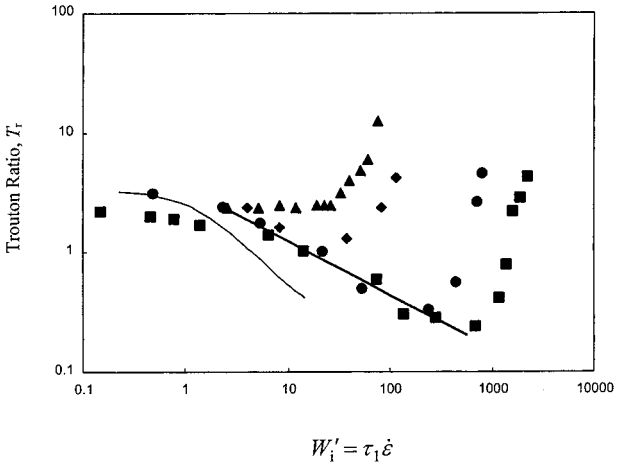

Figure 10. Trouton ratio (T_r) as a function of Weissenberg number ($W_i' = \tau_1\dot{\epsilon}$) for 10 wt % (triangles), 12 wt % (diamonds), 15 wt % (circles), and 20 wt % (squares) solutions. The thick solid line has a slope of −0.45, and the thin solid line is the prediction of Doi−Edwards theory for linear polymers.

et al.[8] In the latter case and at low strains, the solvent contribution dominates, and a well-defined plateau at $T_r^+ \approx 3$ appears. This is followed by an increasing contribution from the unfolding polymer chains at higher strains. Figure 8 does not exhibit a similar plateau because the solvent makes a negligible contribution to the shear viscosity of the solution. The polymer contribution dominates at all strains. The experiments are carried out over a range of strain rates, i.e., from 0.001 to 17 s^{-1}. However, for clarity, only few sample extension rates are presented in this graph. Attempts to run at much higher stretching rates failed due to the filament breakage. For most of the experiments, a steady state was obtained at a strain of approximately 4 units.

Figure 9 shows the steady-state Trouton ratio T_r (open symbols) against Weissenberg number (defined as $W_i = \tau_R\dot{\epsilon}$) for all the solutions. The Rouse times are those evaluated in the previous section and listed in Table 2. In the limit of very low Weissenberg numbers, the Trouton ratio is approximately 3. In this region, the solution behaves as a Newtonian fluid. At very large Weissenberg numbers, chain stretching and retraction compete, and the increase in Trouton ratio suggests that chain stretching is more rapid than chain end fluctuations. In between these two regimes, the extensional viscosity decreases with W_i. Such a decrease in viscosity has also been predicted by the Doi−Edwards model for linear polymers.

There is a significant difference between 10 wt % and the other solutions in that no extension thinning is observed for this solution. Graessley[20] has proposed a classification scheme based on polymer chain dimensions. Under this scheme, the 10% solution is at the boundary between semidilute and concentrated solution, while the more concentrated solutions are in the fully entangled region. It is therefore speculated that the 10% solution is not sufficiently entangled for tube-based theories to be applicable. The minimum in Trouton ratio, for the 12, 15, and 20 wt % solutions, was observed at approximately the same strain rate of 5 s^{-1}. The steady-state extensional stresses (filled symbols) are also shown in Figure 9. At high strain rates, the stresses converge to a single curve. This indicates that the extensional stress, in the limit of high W_i, is only dependent on W_i and points to the dominant role of chain stretching.

Some interesting comparisons can be made between linear polymers and star polymers in order to illustrate the impact of chain topology. For the former reptation is the dominant mechanism and the longest relaxation time is the reptation time, which is larger than the Rouse time by a factor of $3Z$. Hence for linear polymers, one can define a Weissenberg number based on the reptation time $W_{i,d} = \dot{\epsilon}\tau_d$. One may anticipate, according to the Doi−Edwards theory, that the Trouton ratio will decrease below the value of 3 when the strain rate is larger than the inverse reptation time. This corresponds to a Weissenberg number W_i of $1/3Z$. Figure 9 shows that a similar extension thinning region is present in star solutions. However, the onset of this regime occurs at a Weissenberg number 3 orders of magnitude smaller than predicted for linear polymers. For the 20 wt % solution (16.8 entanglements, $3Z \approx 50$ and $1/3Z \approx 0.02$) the extension thinning regime starts at a W_i of about 0.000 02. This is related to the enormous range of time scales that are encountered in star polymer where reptation is absent and chain retraction is the governing mechanism.

When the W_i increases, both the extensional stress and the Trouton ratio increase. The original Doi−Edwards model for linear polymers assumed that the chain retracted instantaneously to their equilibrium length. Marrucci and Grizutti[21] showed that for flows faster than the inverse Rouse time, $W_i \approx 1$, such an assumption is invalid. It appears that a similar effect is present in star polymers, and at high W_i chain stretching contributes to an increase in the stress and Trouton ratio. The onset of chain stretching for stars appears at $W_i \approx 0.1$ compared to $W_i \approx 1$ for linear polymers. The exact reason for this earlier onset is not yet clear.

The longest relaxation time for star polymers can be estimated from eq 13 as the time required for an arm to retract back to the branch point. Figure 10 presents the Trouton ratio data of Figure 9 plotted against the Weissenberg number based on the longest relaxation time (W_i'). For linear polymers, in the region between

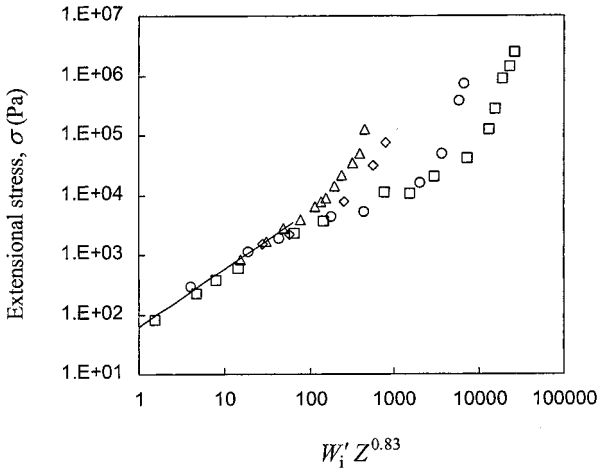

Figure 11. Extensional stress as a function of $W_i'Z^{0.83}$ for 10 wt % (triangles), 12 wt % (diamonds), 15 wt % (circles), and 20 wt % (squares) solutions. The solid line is the prediction of eq 28.

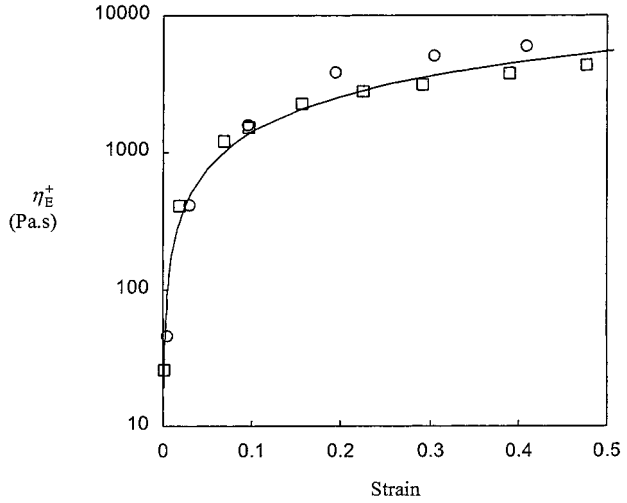

Figure 12. Comparison of the Milner−McLeish model prediction for elongation viscosity growth in the small strain region (solid line) and experimental data (open symbols) for 20 wt % solution. The circles and squares denote the strain rate of 0.5 and 1 s^{-1}, respectively.

$W_{i,d} \approx 1$ and $W_i \approx 1$, the Doi−Edwards theory predicts that the extensional stress remains constant. This implies that the Trouton ratio scales as $W_{i,d}^{-1}$. Note that for star polymers the data in the extension-thinning region superimpose with a slope of −0.45, and this regime starts when the Weissenberg number W_i' exceeds unity (i.e., when the strain rate is larger than the inverse of the longest relaxation time). For comparison, the prediction of the basic Doi−Edwards theory (thin solid line) for a linear polymer is also shown in Figure 10. The Weissenberg number for the Doi−Edwards theory is based on the reptation time. Since τ_1 is much larger than τ_D, this regime for star polymers is much broader than that for linear polymers. Lack of a theory for star polymers makes it difficult to make comparisons on a more quantitative basis.

At very low strain rates, linear viscoelasticity predicts that the Trouton ratio will approach 3. Under these conditions and using eq 25, the extensional stress, at low strain rates, can be shown to be

$$\sigma|_{W_i'\to 0} = 64.7Z^{0.83}W_i' \tag{27}$$

and

$$\sigma|_{W_i'\to 0} = 18.7G_N^{0\ 0.42}W_i' \tag{28}$$

This scaling is quite different from that for linear polymers, where the Doi−Edwards theory predicts that the extensional stress growth is proportional to G_N^0.[1,22] Figure 11 shows the extensional stress as a function of $Z^{0.83}W_i'$. Equation 27 is also plotted in Figure 11 and shows that the model prediction is in good agreement with the experimental data. We may also calculate the transient elongation viscosity growth as 3 times the time-dependent shear viscosity, i.e.,

$$\eta_E^+(t) = 3\int_0^t G(t)\,dt \tag{29}$$

The relaxation modulus of the Milner−McLeish model can be used to predict the start-up behavior in extension of these solutions. Figure 12 shows the comparison of this prediction with experimental data for 20 wt % solution for 0.5 and 1 s^{-1} strain rate. They are in good agreement for small strain $\epsilon < 0.1$. This reinforces the conclusion that the Milner−McLeish model leads to a relaxation modulus that is consistent with extensional data. A more detailed examination will need to await the development of a constitutive model for star polymers.

Concluding Remarks

The rheological properties of entangled solutions of star polymers have been investigated. The Milner−McLeish model is shown to give a very good description of the dynamic data for these solutions. The constants estimated by this model are consistent with independent estimates.

The extensional viscosity of these solutions was measured using the filament stretching rheometer. The extensional viscosity initially decreases with strain rate, and at higher strain rates a region of extension thickening is observed. The results are qualitatively similar to those obtained with solutions of linear polymers. However, for star polymers extensional thinning occurs over 5 decades in strain rate, which is primarily due to the large difference between the longest relaxation time for renewal of chain conformations and the Rouse time for motion of the free ends. In the low strain rate region, the Milner−McLeish model predicts that the extensional stress is proportional to $G_N^{0\ 0.42}$. At high strain rate, the extensional stress is dominated by chain extension and is an unique function of W_i.

Acknowledgment. This work was supported by a program grant from the Australian Research Council. The authors have benefited immensely from discussions with Dr. D. A. Nguyen, Prof. Tom McLeish, Dr. A. E. Likhtman, and Prof. G. H. Mckinley.

References and Notes

(1) Doi, M.; Edwards, S. F. *The Theory of Polymer Dynamics*; Oxford University Press: Oxford, 1986.
(2) Mead, D. W.; Larson, R. G.; Doi, M. *Macromolecules* **1998**, *31*, 7895.
(3) Pearson, D. S.; Helfand, E. *Macromolecules* **1984**, *17*, 888.
(4) Ball, R. C.; McLeish, T. C. B. *Macromolecules* **1989**, *22*, 1911.
(5) Milner, S. T.; McLeish, T. C. B. *Macromolecules* **1997**, *30*, 2159.
(6) Tirtaatmadja, V.; Sridhar, T. *J. Rheol.* **1993**, *37*, 1081.

(7) Sridhar, T.; Tirtaatmadja, V.; Nguyen, D. A.; Gupta, R. K. *J. Non-Newtonian Fluid Mech.* **1991**, *40*, 271.
(8) Gupta, R. K.; Nguyen, D. A.; Sridhar, T. *Phys. Fluids* **2000**, *12*, 1296.
(9) Anna, S. L.; McKinley, G. H.; Nguyen, D. A.; Sridhar, T.; Muller, S. J.; Huang, J.; James, D. F. *J. Rheol.* **2001**, *45*, 83.
(10) Colby, R. H.; Rubinstein, M. *Macromolecules* **1990**, *23*, 2753.
(11) Likhtman, A. E., personal communication, 2000.
(12) Blottiere, B.; McLeish, T. C. B.; Hakiki, A.; Young, R. N.; Milner, S. T. *Macromolecules* **1998**, *31*, 9295.
(13) Milner, S. T.; McLeish, T. C. B.; Young, R. N.; Hakiki, A.; Johnson, J. M. *Macromolecules* **1998**, *31*, 9345.
(14) Cox, W. P.; Merz, E. H. *J. Polym. Sci.* **1958**, *28*, 619.
(15) Menezes, E. V.; Graessley, W. W. *J. Polym. Sci., Part B: Polym. Phys.* **1982**, *20*, 1817.
(16) Yoshida, H.; Shohi, H.; Mikami, Y. *J. Rheol.* **1993**, *37*, 564.
(17) Raju, V. R.; Menezes, E. V.; Marin, G.; Graessley, W. W.; Fetters, L. J. *Macromolecules* **1981**, *14*, 1668.
(18) Graessley, W. W.; Masuda, T.; Roovers, J.; Hadjichristidis, N. *Macromolecules* **1976**, *9*, 127.
(19) Ferry, J. D. *Viscoelastic Properties of Polymer*, 3rd ed.; Wiley: New York, 1980.
(20) Graessley, W. W. *Polymer* **1980**, *21*, 258.
(21) Marrucci, G.; Grizutti, N. *Gazz. Chim. Ital.* **1988**, *118*, 179.
(22) Larson, R. G. *Constitutive Equations for Polymer Melts and Solutions*; Butterworths: Boston, 1988.

MA002192O